A new analytical method for stability analysis of rock blocks with ~~cavity~~ cavities in sub-horizontal strata by the considering eccentricity effect

Xushan Shi[1], Bo Chai[1,3,4], Juan Du[1,2,4], Wei Wang[1,3,4], Bo Liu[1]

[1]School of Environmental Studies, China University of Geosciences, Wuhan, 430078, China
[2]Centre for severe weather and climate and hydro-geological hazards, Wuhan, 430078, China
[3]Hubei Key Laboratory of Yangtze Catchment Environmental Aquatic Science, Wuhan, 430078, China
[4]Research Center for Geohazards Monitoring and Warning in Three Gorges Reservoir, Wanzhou, 404000, China

Correspondence to: Bo Chai (chaibo@cug.edu.cn) and Juan Du (dujuan@cug.edu.cn)

Abstract. The basal cavity of a rock block formed due to differential weathering is an important predisposing factor for rockfall~~,~~ in hard-soft interbedded rocks. ~~The rock~~Rock block falling due to the eccentricity effect with the failure modes of toppling or sliding is defined as biased rockfall in this study. Considering the non-uniform stress distribution due to the eccentricity effect, a new analytical method for three-dimensional stability analysis of biased rockfall is proposed. ~~In addition, a~~A set of factors of safety (Fos) against partial damage (compressive and tensile damage of the soft underlying layer) and overall failure (toppling and sliding of the hard rock block) are used to determine the rockfall susceptibility level. The analytical method ~~was~~ is applied and validated with ~~the~~ biased rockfalls ~~in~~ on the northeast edge of the Sichuan ~~b~~Basin in Southwest China, where ~~a~~ large amounts of rockfalls ~~develops~~have developed, composed of overlying thick sandstone and underlying mudstone. The evolution process of biased rockfalls is divided into four stages, initial state, cavity formation, partial unstable and failure. The proposed method is validated by calculating Fos of the typical unstable rock blocks in the study area. ~~It is indicated that the~~ The continuous retreat of cavity causes ~~the~~ stress redistribution between the hard and soft rock layers. Consequently, the development of the eccentricity effect leads to ~~the~~ damage ~~of~~ to the underlying soft rock layer and ~~the~~ further failure of the hard rock block. The critical cavity retreat ratio is determined ~~as~~ to be 0.33 to classify the low and moderate rockfall susceptibility in the eastern Sichuan Basin. The proposed analytical method is effective for the early identification of biased rockfall, which is significant for rockfall prevention and risk mitigation.

List of symbols

a	length of the block along the x direction
A	area of contact surfaces
b	width of the block along the y direction
c	cohesive force of the mudstone
d_i	width of the basal cavity in a certain direction
e_x	eccentric distance along the x direction

32	e_y	eccentric distance along the y direction
33	E_x	horizontal seismic force along the x direction
34	Fos	factor of safety
35	h	height of the block
36	h_w	height of the water in the fracture
37	H_x	water pressure along the x direction
38	I_x	moment of inertia with respect to the x-axis
39	I_y	moment of inertia with respect to the y-axis
40	k_e	earthquake contribution coefficient
41	k_1	rainfall coefficient, taking 1 in the rainfall scenario and 0 in the non-rainfall scenario
42	k_2	earthquake coefficient, taking 1 in the seismic scenario and 0 in the non-seismic scenario
43	k_3	free surface coefficient, taking 1 for two free surfaces and 0 for three free surfaces
44	M_{bx}	total bending moments with respect to the x-axis on the mudstone foundation
45	M_{by}	total bending moments with respect to the y-axis on the mudstone foundation
46	M_{bEx}	bending moment of E_x with respect to the x-axis on the mudstone foundation
47	M_{bHx}	bending moment of H_x with respect to the x-axis on the mudstone foundation
48	M_{bWx}	bending moment of W with respect to the x-axis on the mudstone foundation
49	M_{Ex}	overturning moment provided by E_x along the x direction
50	M_{Hx}	overturning moment provided by H_x along the x direction
51	M_{px}	stabilizing moment of p_n along the x direction
52	$M_{W_{inx}}$	stabilizing moment provided by W along the x direction
53	$M_{W_{outx}}$	overturning moment provided by W along the x direction
54	N_z	total applied vertical load on the mudstone base
55	O	origin of the (x, y) coordinates
56	$p(x,y)$	pressure magnitude at point (x, y)
57	r_i	the basal cavity retreat ratio equal to the ratio of cavity width to block width in a certain direction
58	W	weight of the block
59	x	distance to O along the x-axis
60	y	distance to O along the y-axis
61	α	true dip of the contact surface
62	γ_s	unit weight of sandstone
63	γ_w	unit weight of water
64	θ_1	apparent dip of α on ~~the~~ plane J1

θ_2	apparent dip of α on ~~the~~ plane J2
σ_{cmax}	ultimate ~~tensile~~ compressive strength of the mudstone
σ_{tmax}	ultimate tensile strength of the mudstone
τ_{max}	ultimate ~~S~~shear ~~S~~strength of the mudstone
φ	friction angle of the mudstone
ω_1	angle between the trend of the contact surface and the x direction
ω_2	angle between the trend of the contact surface and the y direction

1 Introduction

Rockfall is defined as the detachment of a rock block from a steep slope along a surface, on which little or no shear displacement takes place (Cruden and Varnes, 1996). Rockfalls frequently occur in mountainous ranges, cut slopes, and coastal cliffs, and they may cause significant ~~facilities~~ facility damage and casualties in residential areas and transport corridors (Chau et al., 2003; Volkwein et al., 2011; Corominas et al., 2018). Stability ~~and failure probability~~ analysis of rock blocks are crucial for risk management and early warning of rockfall (Kromer et al., 2017).

Rockfall is widespread and poses high risk in the eastern Sichuan Basin, ~~s~~Southwest China (Chen et al., 2008; Chen and Tang, 2010; Zhang et al., 2016; Zhou et al., 2017; Zhou et al., 2018). The rockfall in this area is attributed to the tectonic setting of Jura-type folds and the stratum sequence, which is characterized by the interbedding of hard and soft layers. An alternation of thick sandstone and thin mudstone layers ~~are~~ is formed in the wide and gentle-angle synclines (Zhang et al., 2015; Wu et al., 2018). Weathering is known to be one of the main predisposing factors for rockfall (Jaboyedoff et al., 2021; Zhan et al., 2022). The cliff comprised of hard sandstone is the source of rockfall, and the underlying mudstone is more susceptible to weathering. Along with the ~~extending~~ retreat of basal cavities in the mudstone layer, the gravity centre of the overlying sandstone block moves outward relative to the mudstone. In this case, the stress distribution in the contact surface of sandstone and mudstone is non-uniform. The mudstone on the outer side bears higher compressive stress than that on the inner side. ~~the overlying sandstone blocks gradually become unstable because of the~~ This phenomenon can be defined as an eccentricity effect, which ~~could fail with the mode of~~ leads to mudstone damage and failure of the overlying sandstone by toppling or sliding. This type of rockfall is defined as biased rockfall in this study (Fig. 1). Similar rockfall patterns have been widely reported in other regions, such as Joss Bay in England (Hutchinson, 1972), Okinawa Island in Japan (Kogure et al., 2006), and the Colorado Plateau of the southwestern United States (Ward et al., 2011). ~~Extending~~ Retreat of the basal cavity is a main cause for the failure of the overlying block. Therefore, it is necessary to establish an analytical method, considering the development of the basal cavity, to ~~analyze~~analyse the stress distribution and stability of rock blocks, which is fundamental to the susceptibility assessment and risk control of biased rockfall.

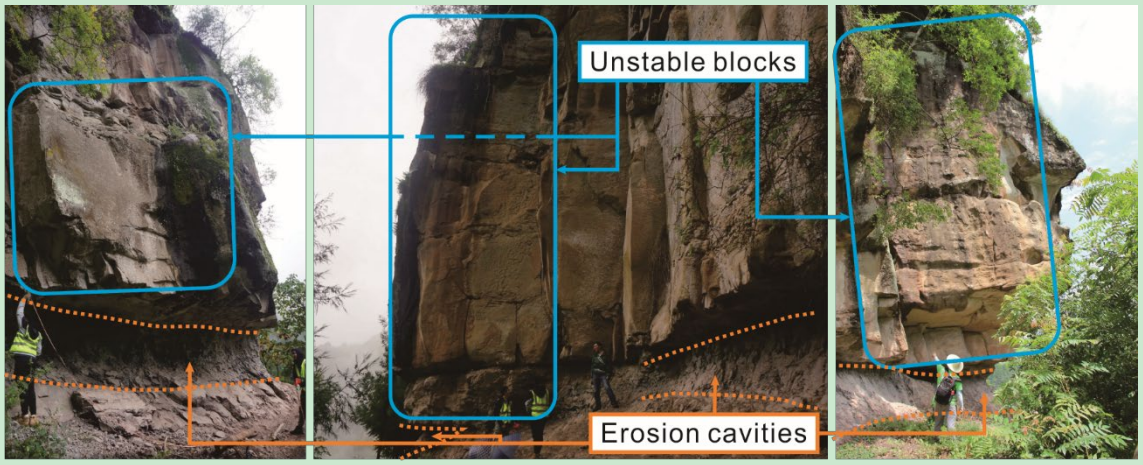

Figure 1 Potential ~~U~~unstable blocks and basal cavities caused by differential weathering.

Rockfall stability analysis methods include statistical analysis (Frattini et al., 2008; Santi et al., 2009), empirical rating systems (Pierson et al., 1990; Ferrari et al., 2016), and mechanical analysis (Jaboyedoff et al., 2004; Derron et al., 2005; Matasci et al., 2018). The statistical analysis and empirical rating systems are suitable for rockfall hazard assessment at a regional scale. The accuracy of statistical analysis depends on the completeness of rockfall inventories (Chau et al., 2003; Guzzetti et al., 2003; D'amato et al., 2016). However, its application to rockfall hazards is limited due to ~~the absence of inventory data~~the lack of complete inventory data (Budetta and Nappi, 2013; Malamud et al., 2004). Empirical and semi-empirical rating systems are used where site-specific rockfall inventories are either unavailable or unreliable. Therefore, rockfall susceptibility can be assessed by heuristic ranking of selected predisposing factors (Frattini et al., 2008; Budetta, 2004). Mechanical analysis based on static equilibrium theory is the main method to ~~analyze~~analyse the stability of site-specific rockfall using the factor of safety (Fos). Ashby (1971) ~~has~~ conducted stability analysis with a parallelepiped block resting on an inclined plane (Fig. 2a), and the solution was subsequently modified by Bray and Goodman (1981)~~,~~ and Sagaseta (1986). Kogure et al. (2006) utilized ~~the~~ a cantilever beam model to determine the critical state of limestone cliffs. Frayssines and Hantz (2009) proposed the limit equilibrium method (LEM) to predict block stability ~~considering~~ against sliding and toppling in steep limestone cliffs (Fig. 2~~b~~c). Chen and Tang (2010) established a stability analysis method of three types of unstable rocks~~,~~ in the Three Gorges Reservoir area with the LEM. Alejano et al. (2015) studied the influence of rounding of block corners on the block stability. Zhang et al. (2016) defined Fos based on fracture mechanics and studied the progressive failure process by ~~analyzing~~analysing crack propagation. Alejano et al. (2010) and Pérez-Rey et al. (2021) deduced ~~the~~ a formula for Fos of blocks with more complex geometry.

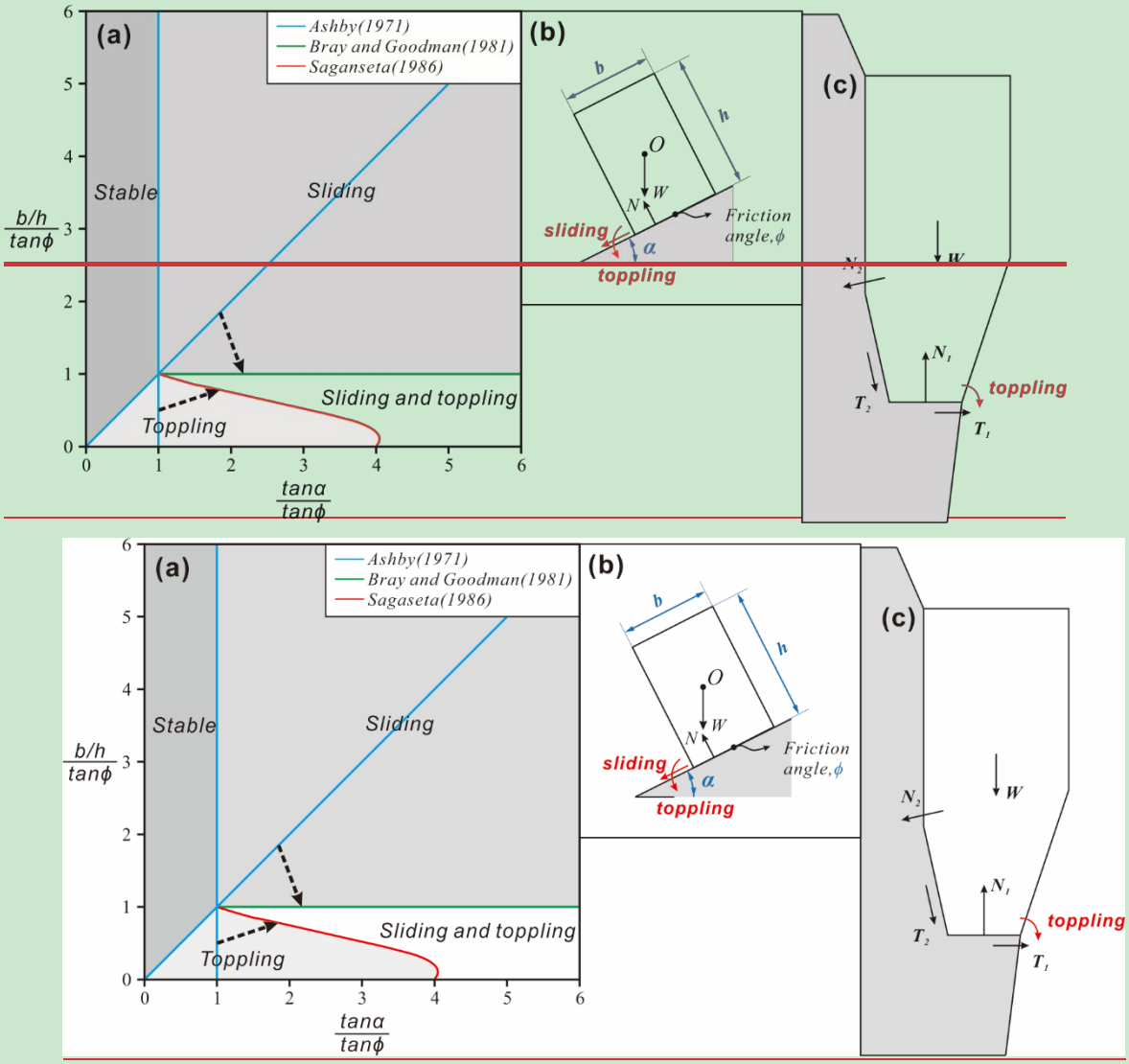

Figure 2 Traditional force analysis diagrams of the rock block. (a) and (b) are stability analysis diagrams of rock blocks ~~in~~ under dynamic conditions, resting on an inclined plane with ~~the~~ a dip angle of α. The rock block is generalized as a cuboid with ~~the~~ dimensions ~~of b × h~~ *b* × *h* and weight *W* (as modified from Ashby (1971), Bray and Goodman (1981) and Sagaseta (1986)). (c) Force description of the toppling model proposed by Frayssines and Hantz (2009). In the above assumptions, *N*, *T*, and *W* are~~is~~ regarded as ~~a~~ forces applied at a point.

The supporting force ~~at~~ on the contact surface is assumed to be applied at a point in the current LEM methods (i.e., N in Fig. 2 b and c). However, the supporting force is actually a distributed force. The cavity generates an eccentricity effect on the overlying rock ~~mass~~ block and results in a non-uniform distribution of the supporting force on the contact surface, which is not considered in the traditional LEM. Furthermore, most studies simplified the three-dimensional geometry of the ~~slope~~ rock block by one cross-section, which is used to represent the critical features of the slope structure. Nevertheless, for natural blocks with basal cavities ~~(Pérez-Rey et al., 2021)~~, the cavities usually present different depths along different

directions ~~usually present different depths~~(Pérez-Rey et al., 2021). Therefore, a three-dimensional model is necessary to calculate the accurate stability. ~~Besides~~In addition, when a block has multiple free faces and a complex structure, ~~it's~~ its potential failure ~~will be~~is dominated by different modes, including rock mass damage and overall block failure. Therefore, the probable failure modes should be determined prior to the calculation of Fos.

Based on rockfall investigation in the Eastern Sichuan Basin, China, the main objective of this study was to propose a new three-dimensional method for the determination of failure modes and Fos of biased rockfall, considering the non-uniform force distribution on the contact surfaces. Compared with the traditional LEM method, this study takes into account the partial damage of the underlying soft rock and the overall instability of the overlying hard rock blocks, and can evaluate the stability of biased rockfall more comprehensively. Fos of the typical unstable rock blocks in the study area ~~were~~ are calculated to validate the ~~new~~ proposed method. In addition, the critical cavity retreat ratio ~~(r)~~ in this area ~~was~~ is ~~given~~analysed. This study is an extension of the basic LEM for rockfall, which ~~could~~ can promote the accuracy of rockfall stability analysis and facilitate rockfall prevention and risk mitigation.

2 Study area

2.1 Geological setting

The study area is located ~~in~~ on the northeastern edge of the Sichuan ~~b~~Basin, China (Fig. 3a). Continuous erosion processes generate moderate-low mountain and valley landforms (Yu et al., 2021). The tectonic structure of this area is characterized by a series of ~~NEE~~ ENE anticlines and synclines (Fig. 3b, c). In the anticline~~s~~ area, the rock layers dip relatively steeply, where translational rockslides ~~is~~ are the main mode of slope failure. The syncline area is dominated by ~~gentle~~ gently dipping strata and is prone to rockfall (Zhou et al., 2018). The study area is located in the core of the Matouchang syncline, where the rock layers are sub-horizontal (Fig. 3d, e). In this valley, due to the longstanding fluvial incision, the relative relief is ~~about~~ approximately 500 m and the valley flanks are extremely steep (Fig. 3e). ~~Besides~~In addition, the toes of the hill slopes are reshaped because of the construction of the G318 national road, which is the main traffic line and is always threatened by rockfalls dropping from ~~the~~ steep rock slopes (shown in Fig. 3d and Table 1).

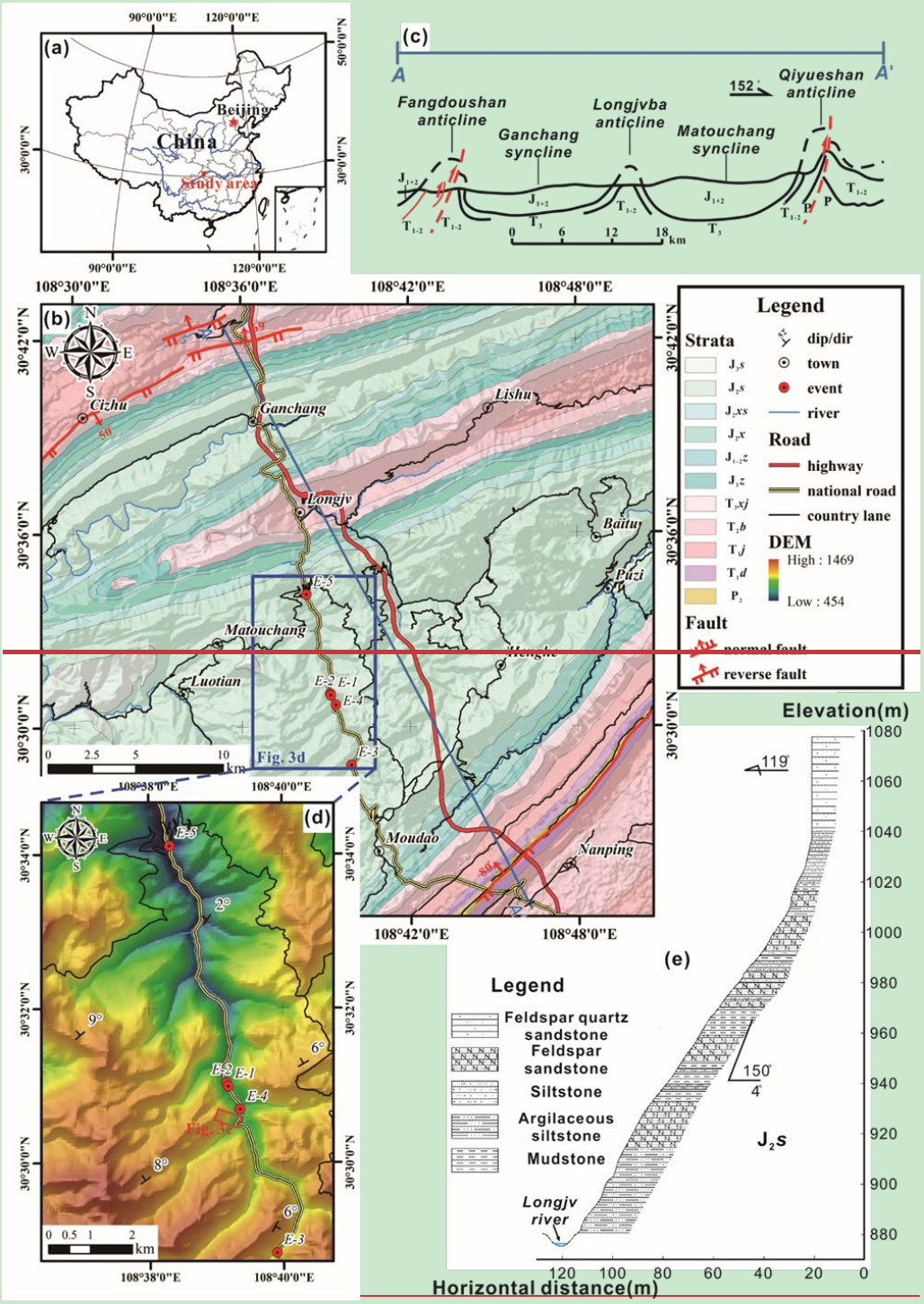
(a)
China
Beijing
Study area
90°0'0"E
120°0'0"E
30°0'0"N
(c)
A
A'
152°
Qiyueshan anticline
Fangdoushan anticline
Ganchang syncline
Longjvba anticline
Matouchang syncline
0 6 12 18 km
(b)
108°30'0"E
108°36'0"E
108°42'0"E
108°48'0"E
30°42'0"N
30°36'0"N
30°30'0"N
Cizhu
Ganchang
Lishu
Longjv
Baitu
Paizi
Matouchang
Luotian
Hengshe
Moudao
Nanping
E-1
E-2
E-3
E-4
E-5
Fig. 3d
0 2.5 5 10 km
Legend
Strata
dip/dir
town
event
river
Road
highway
national road
country lane
DEM
High : 1469
Low : 454
Fault
normal fault
reverse fault
(d)
108°38'0"E
108°40'0"E
30°34'0"N
30°32'0"N
30°30'0"N
Fig. 3c
0 0.5 1 2 km
(e)
Elevation(m)
Horizontal distance(m)
Legend
Feldspar quartz sandstone
Feldspar sandstone
Siltstone
Argilaceous siltstone
Mudstone
Longjv river
J2s
119°
150°
4°

150

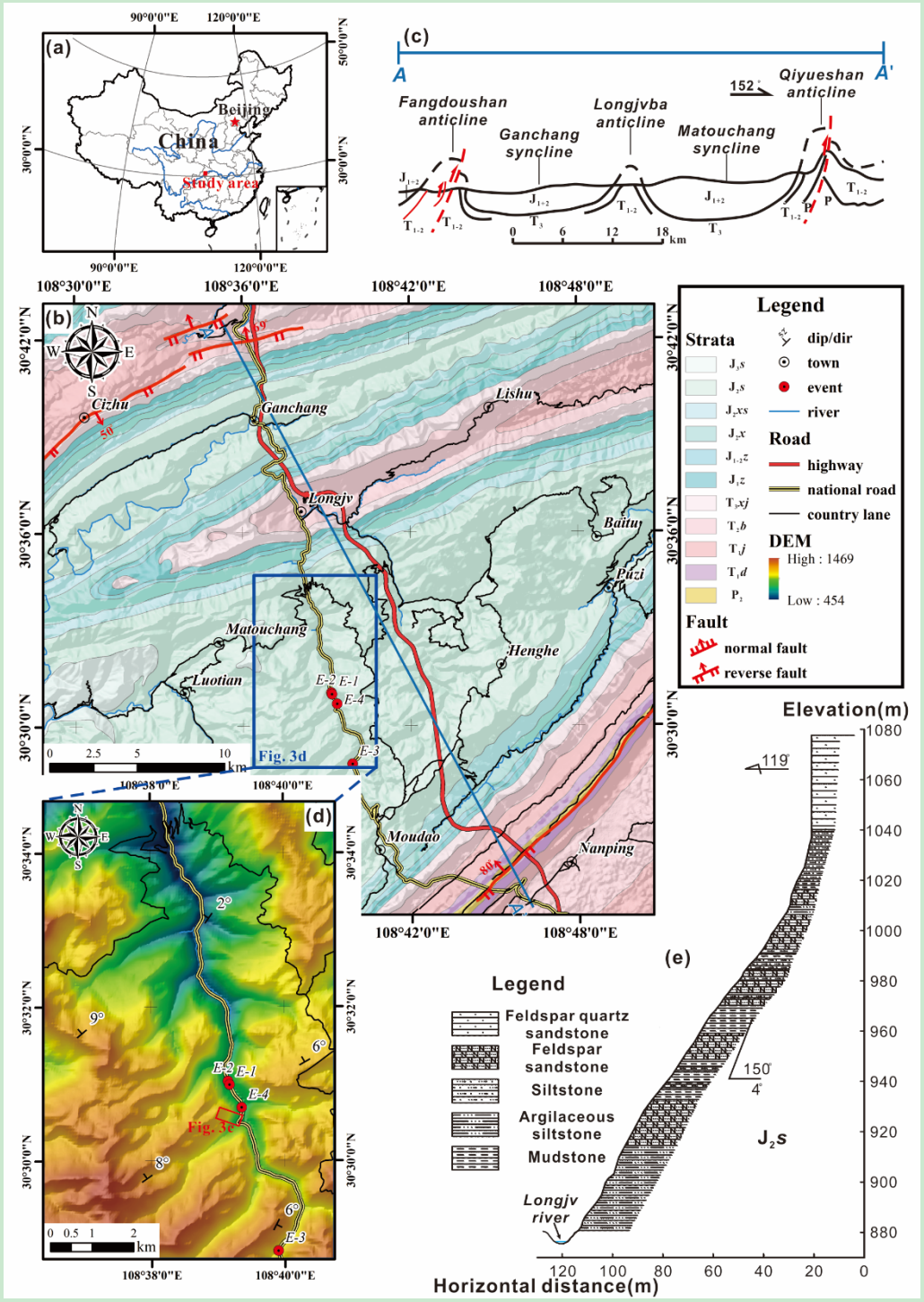

Figure 3 (a) Location of the study area in China; (b) geological map of the study area; (c) tectonic sketch profile of A-A'~~;~~, whose location is showed in Fig. 3b; (d) rockfall-prone segment and key investigation areas. The red dots are the positions of historical rockfall events,

corresponding to the ~~serial~~ numbers in Table 1; (e) Geological cross-section of the hillslope in the Jitougou section of G318 national road, which is marked by a red rectangle in Fig. 3d.

Table 1 Historical rockfall events along G318 national road in the study area

~~Serial number~~No	Location	Time of occurrence (GMT+8)	Volume [m^3]	Consequence
E-1	K1698+900	2014-05 to 06*	Unknown	The power transmission facilities outside the road were smashed.
E-2	K1699+000	2015-02-14 23:00	About 240	A passing truck was stuck and two people dead.
E-3	K1690+700	2015-06-16	Unknown	The road was interrupted for a day.
E-4	K1698+400	2015-06-18 09:00	About 200	A vehicle was crashed into a gully and four people dead.
~~E-5~~	~~K1741+800~~	~~2020-04-21 05:30~~	~~About 232000~~	~~Eight houses were damaged and a gas station was affected.~~

*Note: The exact time is unknown.

2.2 Rockfall characteristics

The slopes in the study area ~~have multi-layer unstable rock blocks (Fig. 4a), which are~~ consist of a sub-horizontally interbedded~~interbedding of~~ sandstone and mudstone layer~~s~~. Therefore, there are multiple layers of potentially unstable rock blocks in the hill slopes (Fig 4a). The thick sandstone has two sets of sub-vertical joints (Fig. 5), which cut the rock mass into blocks as the potential rockfall source (Fig. 4b). Cavities ~~are~~ have formed in the underlying mudstone layer (Fig. 4c, d). Joints and bedding planes (BP) constitute the detachment surfaces between the blocks and steep slope (Fig. 4e). The ~~E~~eccentricity effect produced by the mudstone cavity plays an important role in the ~~rockfall~~ evolution process of rockfall. When the basal mudstone cannot provide adequate supporting force, the blocks detach from the steep slope, and biased rockfall occurs. ~~There are two possible failure modes of biased rockfall, namely s~~Sliding and toppling are two possible failure modes of biased rockfall.

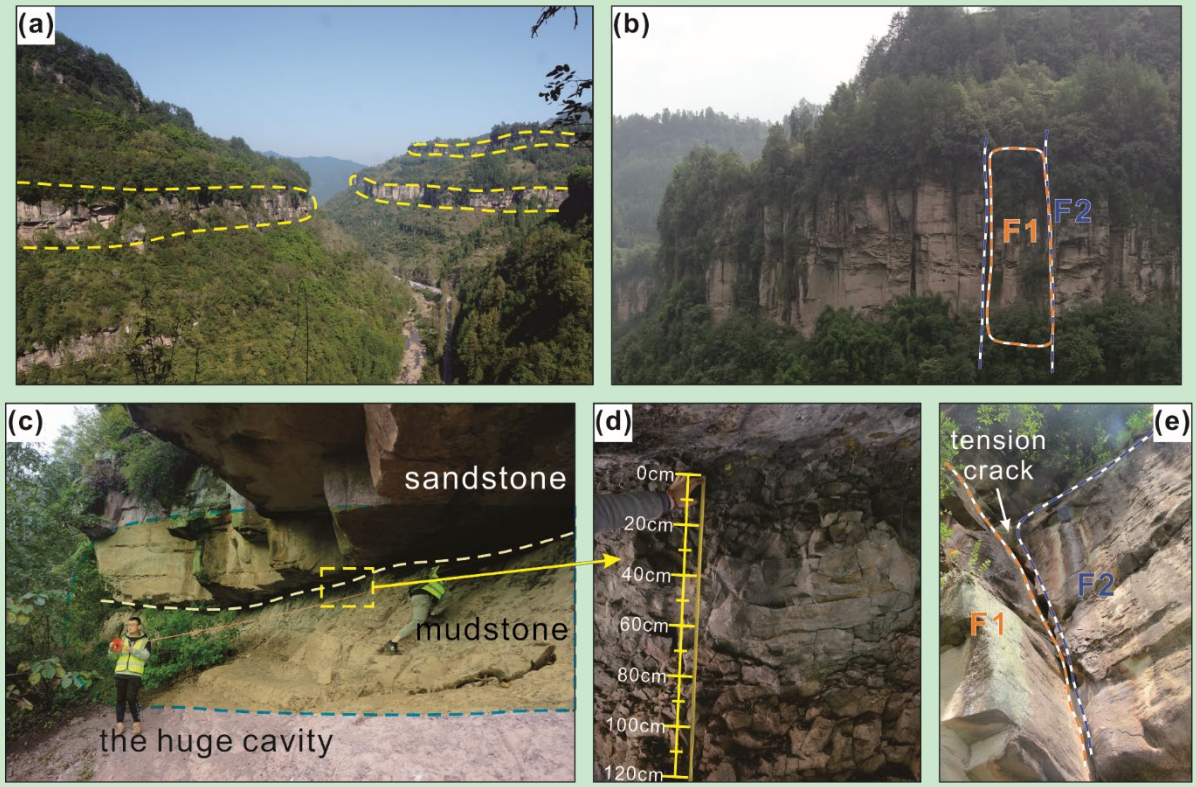

Figure 4 Characteristics of biased rockfalls in the study area. (a) Multiple-layers~~Multi-layer~~ of rockfall sources, which is consist of thick sandstone. (b) Two sets of sub-vertical joints (F1 and F2) recognized by the UAV photos. (c) ~~A l~~Large basal cavity developed in the underlying mudstone. (d) ~~The d~~Dense fractures on the mudstone surface generated by weathering and compression. (e) ~~A v~~Vertical tension crack in the rear of the block, through which precipitation can infiltrate.

~~In the study area, rainfall is the main predisposing factors of rockfall.~~ According to the historical rockfall events in this area, precipitation is considered a triggering effect of rock instability. The precipitation mainly infiltrates along the sub-vertical joints or cracks of the sandstone (Fig. 4e). However, the ~~draining~~ drainage of fissure water is hysteretic due to the obstruction of basal mudstone. Therefore, transient steady flow exists in vertical cracks during heavy rainfall, and the hydrostatic pressure triggers the detachment of rock blocks. Thus, typical scenarios (such as rainfall intensity and earthquake) need to be considered in the stability analysis model.

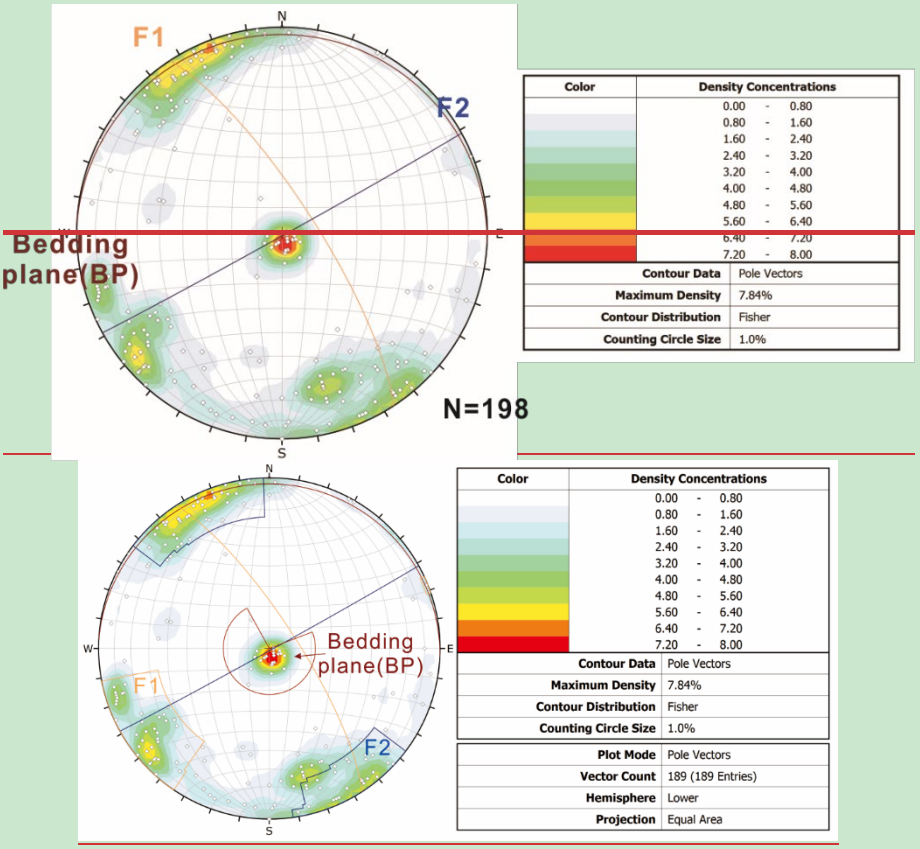

Figure 5 Stereo net produced using compass-clinometer survey data, which shows the densities and orientations of five clusters. The data were collected in the rockfall-prone area shown in Fig. 3d.

3 Calculation method

3.1 Geological models and assumptions

A detailed geological investigation ~~for~~ of unstable rock blocks ~~were~~ was carried out in the study area (Fig. 6). The geological model of the rock block is mainly composed of the overlying sandstone and the underlying mudstone. The sandstone block is assumed to be a rigid body, which is divided by two sets of orthogonal vertical smooth joints without friction resistance. According to the relatively persistent sub-vertical fractures observed in the field, the vertical joints are assumed to be fully persistent in the geological model. ~~Blocks with multiple free faces are prone to failure.~~The sandstone block is assumed to be a complete body without persistent discontinuity, and it will not disintegrate before it falls. Due to the cavity in ~~the~~ mudstone, the contact surface between sandstone and mudstone ~~has~~ exhibits an eccentricity effect~~. The underlying mudstone plays the role of a rectangular base, which provides~~ where non-uniform ~~distributed forces~~ stresses are distributed at different ~~locations~~positions. ~~Mudstone is loaded by compressive stress, tensile stress and shear stress, however, it doesn't present~~

~~deformation.~~ Mudstone is mainly loaded by compressive stress and tensile stress. When the compressive stress of mudstone exceeds its strength on the outer side, some initial damage appears. The effective contact surface between mudstone and sandstone is reduced, which aggravates the non-uniform distribution of stress. In this way, the ability of mudstone to resist the sliding and toppling of overlying sandstone is reduced. In the field, compression deformation of mudstone can be observed, which usually manifests as micro-fractures and cleavages (Fig. 4d). The deformation is very slight and slow in the short term. In addition, the LEM is essentially a force/stress approach that does not take into account the deformation. Therefore, in this study, it is assumed that the mudstone is not subjected to deformation. The rock block ~~keeps~~ remains in the state of static equilibrium prior to the final overall failure. Fig. 7 ~~expresses~~ displays the four evolution stages of biased rockfall. In the initial stage, the base cavity has not yet formed, and the normal force acting on the contact surface is uniform in different positions. The ~~E~~eccentricity effect leads to a non-uniform supporting force as the cavity grows, and partial~~ly~~ damage gradually develops ~~until~~ when the non-uniform ~~force~~ stress exceeds the compressive or tensile strength of the mudstone. Under the triggering effects of rainfall or earthquakes, the rock blocks ~~will be~~are separated by sliding or toppling.

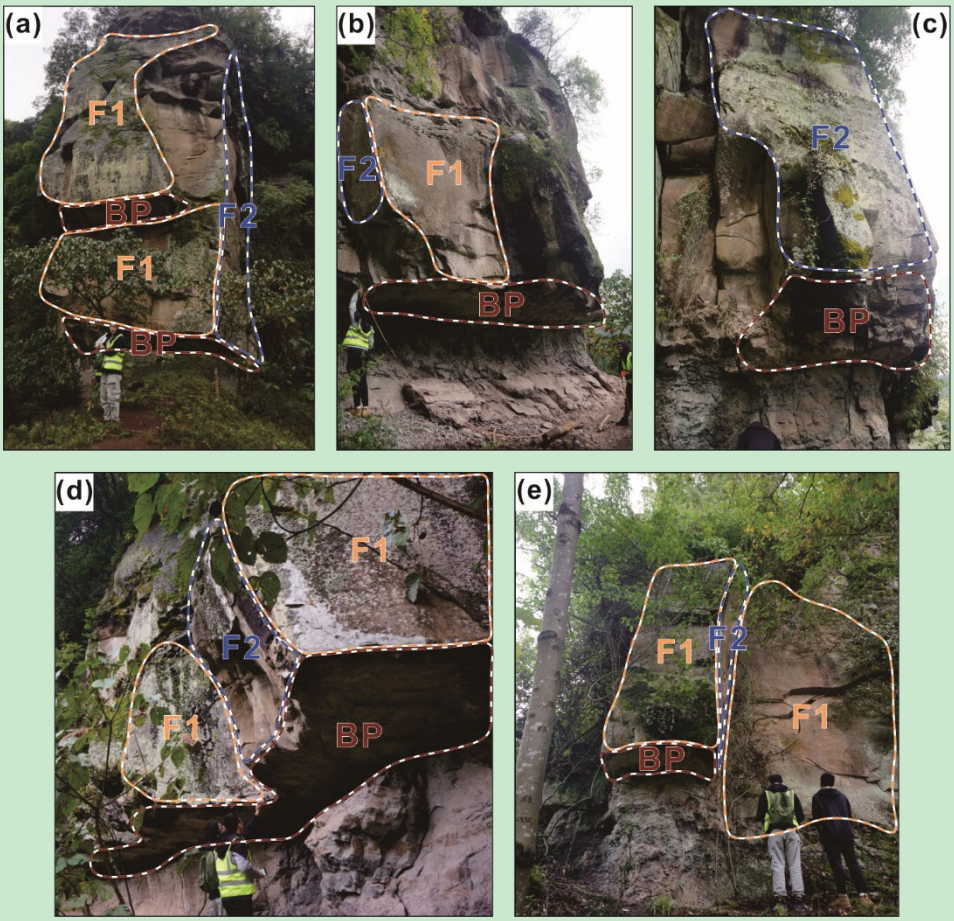

Figure 6 The unstable blocks were labelled W02, W08, W18, W04, and W21, which are detached by the ~~dominated~~ dominating discontinuities in Fig. 5. ~~Obvious b~~Basal cavities can be identified under the bedding planes of sandstone.

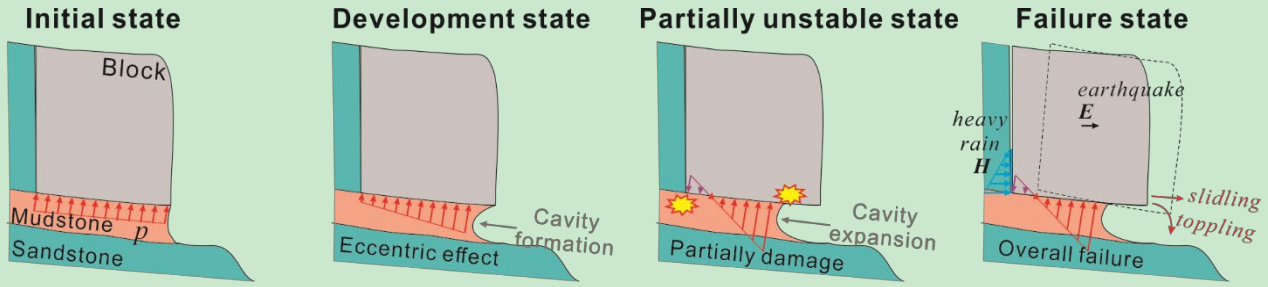

Figure 7 The evolution process of rock blocks from stable state to failure.

Fig. 8 represents the mechanical model of the force equilibrium analysis of a rock block with two or three free faces. The rock block (the overlying sandstone) is generalized as a parallelepiped block. The underlying mudstone is impermeable, so rainfall can fill the joints and transmit horizontal hydrostatic pressure. The shear strength of the underlying mudstone is assumed to obeys the Mohr–Coulomb~~Mohr Coulomb~~ criterion. ~~The predisposing factors s of r~~Rainfall and earthquakes decrease Fos by generating hydrostatic pressure H in the vertical crack and horizontal seismic force E on the block.

A Cartesian coordinate system is established in three-dimensional space for the force analysis. The origin O is located at the centre of the contact surface between sandstone and mudstone. For the case with two free surfaces, the orientation of the free surfaces is set to be the positive direction of the x-axis and y-axis. For the case with three free surfaces, the negative direction of the x-axis is also a free surface. Joint J2 is perpendicular to the x-axis, and joint J1 is perpendicular to the y-axis.

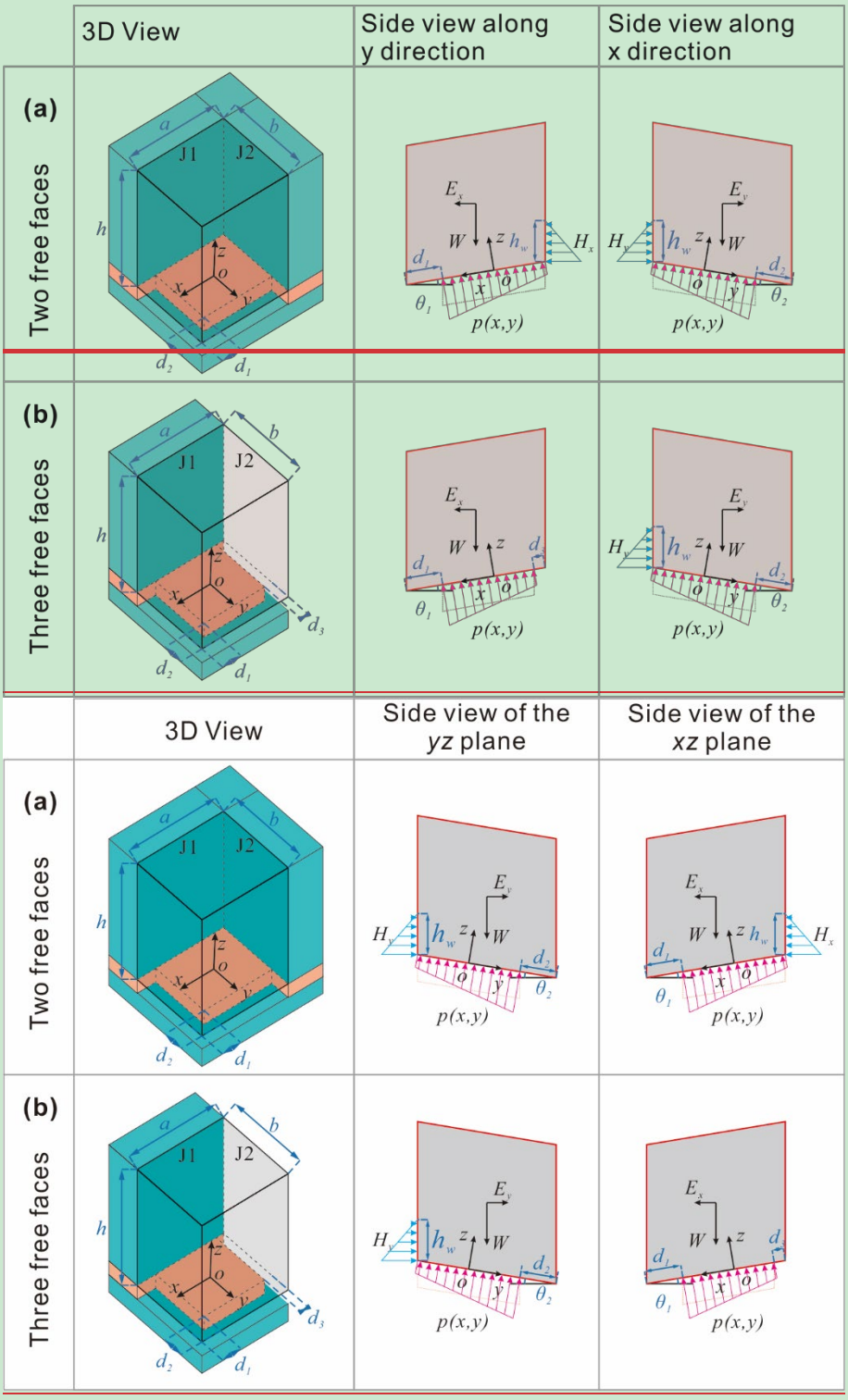
3D View
Side view along y direction
Side view along x direction
(a)
Two free faces
(b)
Three free faces
J1
J2
3D View
Side view of the yz plane
Side view of the xz plane
p(x,y)

220

221

Figure 8 Diagram of the force equilibrium analysis of the rock block model. (a) and (b) represent the case of unstable rock blocks with two or three free vertical surfaces, respectively.

3.2 Calculation processes

3.2.1 ~~Distributed force~~Stress distribution at the block base

The following formulas are used to calculate the apparent dip of α (θ_1 and θ_2):

$$\theta_1 = \arctan(\tan\alpha \cdot \cos\omega_1) \tag{1}$$

$$\theta_2 = \arctan(\tan\alpha \cdot \cos\omega_2) \tag{2}$$

~~Where,~~ where ω_1 and ω_2 are the angles between the trend of the contact surface and the x direction or y direction, respectively.

As shown in Fig. 8b, with respect to the x-axis, gravity, seismic forces, and hydrostatic pressure create a ~~bending moments~~ non-symmetrical stress distribution on the foundation. The bending moment of gravity with respect to the x-axis (M_{bWx}) is

$$M_{bWx} = W \cdot \frac{d_1 - d_3}{2}\cos\theta_1 \tag{3}$$

~~Assume~~ Assuming that the height of the water in the fracture is h_w, the hydrostatic pressure along the x direction (H_x) and its bending moment (M_{bHx}) are respectively expressed as~~,~~

$$H_x = \frac{\gamma_w h_w^2}{2}(b - d_2) \tag{4}$$

$$M_{bHx} = \int_{-\frac{b-d_2}{2}}^{\frac{b-d_2}{2}} \int_0^{h_w\cos\theta_1} \gamma_w \left(h_w - \frac{z}{\cos\theta_1}\right)\left(\frac{z}{\cos\theta_1} + \frac{a - d_1 - d_3}{2} \cdot \sin\theta_1\right) dz dy \tag{5}$$

The horizontal seismic force along x direction (E_x) and its bending moment (M_{bEx}) are respectively expressed as~~,~~

$$E_x = k_e W \tag{6}$$

$$M_{bEx} = E_x\left(\frac{h}{2} - \frac{d_1 - d_3}{2}\sin\theta_1\right) \tag{7}$$

The total applied vertical load (N_z) and the total bending moments along the x direction (M_{bx}) can be derived as~~,~~

$$N_z = W\cos\alpha - (H_x \cdot k_1 \cdot k_3 + E_x \cdot k_2)\sin\theta_1 - (H_y \cdot k_1 + E_y \cdot k_2)\sin\theta_1 \tag{8}$$

$$M_{bx} = M_{bWx} + M_{bHx} \cdot k_1 \cdot k_3 + M_{bEx} \cdot k_2 \tag{9}$$

~~Under natural condition, k_1 and k_2 are both equal to 0. Under rainfall conditions, $k_1 = 0$. Under earthquake conditions, $k_2 = 0$. For the case of two free faces, $k_3 = 1$; for the case of three free surfaces, $k_3 = 0$.~~where k_1, k_2 and k_3 are the coefficients set to make Eq. (8) and Eq. (9) compatible with different calculation scenarios. Therefore, Eqs. (8) and (9) and the following formulas can be expressed in a unified form. In the natural scenario, k_1 and k_2 are both equal to 0. In the rainfall scenario, $k_1 = 1$. In the earthquake scenario, $k_2 = 1$. For the case of two free faces, $k_3 = 1$. For the case of three free surfaces, $k_3 = 0$.

Based on bending theory (Adrian, 2010), the eccentricity distance along the x direction (e_x) can be expressed as~~,~~

$$e_x = \frac{M_{bx}}{N_z} = \frac{M_{bWx} + M_{bHx} \cdot k_1 \cdot k_3 + M_{bEx} \cdot k_2}{W \cos\alpha - (H_x \cdot k_1 \cdot k_3 + E_x \cdot k_2) \sin\theta_1 - (H_y \cdot k_1 + E_y \cdot k_2) \sin\theta_1} \tag{10}$$

The same method can be used to obtain e_y~~,~~:

$$e_y = \frac{M_{by}}{N_z} = \frac{M_{bWy} + M_{bHy} \cdot k_1 + M_{bEy} \cdot k_2}{W \cos\alpha - (H_x \cdot k_1 \cdot k_3 + E_x \cdot k_2) \sin\theta_1 - (H_y \cdot k_1 + E_y \cdot k_2) \sin\theta_1} \tag{11}$$

According to the stress distribution of a rectangular shaped foundation (Adrian, 2010), the stress in the (x, y) coordinates, $p(x, y)$, ~~results to be~~is~~,~~

$$p(x,y) = \frac{N}{A} + \frac{Ne_x}{I_y}x + \frac{Ne_y}{I_x}y \tag{12}$$

~~W~~with the formulas~~,~~

$$I_x = \frac{(a-d_1)(b-d_2)^3}{12} \tag{13}$$

$$I_y = \frac{(b-d_2)(a-d_1)^3}{12} \tag{14}$$

$$A = (a - d_1 - d_3)(b - d_2) \tag{15}$$

~~b~~By substituting Eq. (13-15) into Eq. (12), $p(x, y)$ can be derived as~~,~~

$$p(x,y) = \frac{N}{A}\left[1 + \frac{12e_x}{(a-d_1-d_3)^2}x + \frac{12e_y}{(b-d_2)^2}y\right] \quad x \in \left[-\frac{a-d_1-d_3}{2}, \frac{a-d_1-d_3}{2}\right], y \in \left[-\frac{b-d_2}{2}, \frac{b-d_2}{2}\right] \tag{16}$$

p_{max} and p_{mim} can be derived from Eq. (16) as~~,~~

$$p_{max} = p\left(\frac{a-d_1-d_3}{2}, \frac{b-d_2}{2}\right) \tag{17}$$

$$p_{min} = p\left(-\frac{a-d_1-d_3}{2}, -\frac{b-d_2}{2}\right) \tag{18}$$

The mudstone foundation has both ~~the~~ compressive strength and tensile strength, so the value of $p(x, y)$ is modified to obtain the two piecewise functions~~,~~

$$p_p(x,y) = \begin{cases} \sigma_{cmax}, & p(x,y) \geq \sigma_{cmax} \\ p(x,y), & 0 < p(x,y) \leq \sigma_{cmax} \\ 0, & p(x,y) < 0 \end{cases} \tag{19}$$

$$p_n(x,y) = \begin{cases} 0, & p(x,y) < -\sigma_{tmax} \\ p(x,y), & -\sigma_{tmax} \leq p(x,y) < 0 \\ 0, & p(x,y) \geq 0 \end{cases} \tag{20}$$

Here, $p_p(x, y)$ provides support normal force for the ~~underlying~~ overlying sandstone, and $p_n(x, y)$ provides tension force.

3.2.2 Calculation of factors of safety

According to the principle of friction, the ultimate ~~S~~shear ~~S~~strength τ_{max} ~~results to be,~~is

$$\tau_{max} = \int_{-\frac{a-d_1-d_3}{2}}^{\frac{a-d_1-d_3}{2}} \int_{-\frac{b-d_2}{2}}^{\frac{b-d_2}{2}} \left[p_p(x,y)\tan\varphi + c\right] dy\, dx \tag{21}$$

Therefore, ~~the~~ Fos against sliding, Fos_{sl}, can be defined as~~,~~

$$Fos_{sl} = \frac{S_{stabilizing}}{S_{sliding}} = \frac{\tau_{max}}{W|\sin\alpha_s| + H_x \cdot \cos\omega_s \cdot \cos\alpha_s \cdot k_1 \cdot k_3 + H_y \cdot |\sin\omega_s| \cdot \cos\alpha_s \cdot k_1 + E \cdot \cos\alpha_s \cdot k_2} \tag{22}$$

When the block can slide freely, $\alpha_s = \alpha$, $\omega_s = 0$; when the block is constrained to slide along a joint plane (e.g., J1), $\alpha_s = \theta_1 \ or \ \theta_2$, $\omega_s = \omega_1 \ or \ \omega_2$. For the case of an anaclinal slope, the sliding direction is opposite to the free surface. Therefore, the rock block does not slide, and Fos_{sl} is not ~~exist~~ considered in the model.

With regard to stability against toppling, along the x direction, the part of the block above the mudstone base provides the stabilizing moment $M_{W_{inx}}$, and the part of the block above the cavity provides the overturning moment $M_{W_{outx}}$. When ~~the~~ tension exists, there ~~will be~~is an additional stabilizing moment. M_{px}, $M_{W_{inx}}$, $M_{W_{outx}}$ and M_{px}can be derived as~~,~~

$$M_{W_{inx}} = W\frac{a-d_1}{a}\cos\theta_1 \cdot \left(\frac{a-d_1}{2}\right) \tag{23}$$

$$M_{W_{outx}} = W\frac{d_1}{a}\cos\theta_1 \cdot \frac{d_1}{2} \tag{24}$$

$$M_{px} = -\int_{-\frac{b-d_2}{2}}^{\frac{b-d_2}{2}} \int_{-\frac{a-d_1-d_3}{2}}^{\frac{a-d_1-d_3}{2}} p_n(x,y) \cdot \left(\frac{a}{2} - d_1 - x\right) dx\, dy \tag{25}$$

~~A~~and M_{Hx}~~,~~and M_{Ex} can be derived as~~,~~

$$M_{Hx} = \int_{-\frac{b-d_2}{2}}^{\frac{b-d_2}{2}} \int_0^{h_w\cos\theta_1} \gamma_w \left(h_w - \frac{z}{\cos\theta_1}\right)\left(\frac{z}{\cos\theta_1} + (a-d_1)\sin\theta_1\right) dz dy \tag{26}$$

$$M_{Ex} = E_x\left(\frac{h}{2} + \left(\frac{a}{2} - d_1\right)\sin\theta_1\right) \tag{27}$$

Therefore, the Fos against toppling along the x direction, Fos_{tox}, results ~~to be,~~in

$$Fos_{tox} = \frac{M_{stabilizing}}{M_{overturning}} = \frac{M_{W_{inx}} + M_{px}}{M_{W_{outx}} + M_{Hx} \cdot k_1 \cdot k_3 + M_{Ex} \cdot k_2} \tag{28}$$

Similarly, ~~the~~ Fos_{toy} can be obtained as~~,~~

$$Fos_{toy} = \frac{M_{stabilizing}}{M_{overturning}} = \frac{M_{W_{iny}} + M_{py}}{M_{W_{outy}} + M_{Hy} \cdot k_1 + M_{Ey} \cdot k_2} \tag{29}$$

The smaller value is selected as the Fos of the toppling failure mode~~,~~ Fos_{to}~~:~~:

$$Fos_{to} = min\left(Fos_{tox}, Fos_{toy}\right) \tag{30}$$

When the stress on mudstone exceeds its strength~~s~~, it ~~has~~ causes partial damage and decrease~~s~~ the stability of the rock block.

Therefore, ~~the~~ Fos with the consideration of compressive strength (Fos_{co}) and tensional strength (Fos_{te}) can be derived as~~,~~

$$Fos_{co} = \frac{\sigma_{~~tc~~max}}{p_{max}} \tag{31}$$

$$Fos_{te} = \frac{\sigma_{etmax}}{-p_{min}} \quad (32)$$

Fos_{co} and Fos_{te} represent the current damage degree of mudstone due to compressive stress and tensile stress, respectively. When the stress exceeds the ultimate strength, the strength of the mudstone is reduced to the residual value, and the initial deformation appears. The ability of mudstone to provide resistance to the sliding and toppling of sandstone blocks is thus reduced, and Fos_{sl} and Fos_{to} subsequently decline. The smaller the value of Fos_{co} and Fos_{te}, the greater the damage to the underlying mudstone. The effective contact area between sandstone and mudstone becomes smaller as the development of compressive and tension damage, which significantly affects the stability of the overlying sandstone block.

Finally, four Fos of unstable rock block ~~were~~ are obtained. Fos_{sl} and Fos_{to} are routine indicators directly ~~about~~ representing the stability of sandstone blocks ~~that directly characterize its stability~~. Fos_{co} and Fos_{te} are two indicators proposed in this study~~,~~ for the stability analysis of biased rockfall, which describe the damage state of the underlying mudstone base. It is necessary to ~~aggregate~~ simultaneously consider four Fos to ~~judge~~ evaluate the stability of unstable biased rockfall~~rock mass~~. The entire calculation process is shown in Fig. 9.

Figure 9 ~~The c~~Calculation process of Fos of the unstable rock blocks.

4 Parameters and results

A detailed field investigation was carried out in the source area of rockfall (Fig. 3d ~~and 4a~~). The size of the blocks ~~is~~ was determined by on-site measurement with tape and a laser rangefinder. The basal cavities in mudstone were measured with a steel ruler, and the morphological characteristics of mudstone foundation ~~are~~ were mainly described with the average erosion depth of the cavity. The attitude of discontinuities was measured by compass. The mechanical parameters for the Fos calculation of rock blocks ~~are~~ were ~~abundantly recorded in~~ determined by referring to published literature and ~~the~~ investigation reports ~~and published literatures~~ in this area. The unit weight of the sandstone block (γ_s) is 25 kN/m^3 (Tang et al., 2010), the friction angle of the contact surface (φ) is set to ~~be~~ 25°~~°~~ and the cohesion (c) is set to ~~be~~ 70 kPa (Zhang et al., 2016). Because of the strength degradation of mudstone foundations due to intense ~~weathered~~weathering, the maximum compressive stress of mudstone (σ_{cmax}) is replaced by the bearing capacity of mudstone foundations (2300 kPa), which is obtained through plate load tests in adjacent areas (Zheng et al., 2021). ~~Besides~~In addition, the maximum tensile stress of mudstone (σ_{tmax}) is value as ~~one~~ one-ninth of σ_{cmax}. The height of the water level (h_w) is set to be one-third of h, and an earthquake contribution coefficient k_e of 0.05 is considered in stability calculations. The data obtained from the field survey were organized according to the coordinate system of the geological model in Section 3.1, and Fos was calculated according to the calculation steps in Section 3.2. The calculated geometric parameters and Fos results are shown in Table 2.

Table 2 Geometric parameters of rock blocks in the study area and Fos results ~~obtained from the analytical method in section 3~~.

Block number	Free faces	h [m]	a [m]	b [m]	d_1 [m]	d_2 [m]	d_3 [m]	α [°]	Dip direction [°]			NS (Natural scenario)					RS (Rainfall scenario)				ES (Earthquake scenario)			
									BD	J1	J2	Fos_{te}	Fos_{co}	Fos_{sl}	Fos_{to}	Fos_{min}	Fos_{te}	Fos_{co}	Fos_{sl}	Fos_{to}	Fos_{te}	Fos_{co}	Fos_{sl}	Fos_{to}
W01	3	23	7.2	6.1	0.65	0.25	0.17	6	78	7	97	-	2.99	5.61	101.54	2.99	-	2.56	3.18	11.91	0.90	1.63	3.81	4.88
W02	3	23	6.42	5.25	0.78	0.4	0.31	16	148	51	141	-	2.84	2.10	52.28	2.10	-	2.33	1.54	8.49	0.51	1.48	1.82	3.79
W03	2	20	3.5	2.6	0.84	0.55	-	7	341	53	143	0.52	1.56	16.53	4.72	0.52	0.15	0.86	2.83	1.02	0.14	0.81	9.12	1.01
W04	2	19	4.6	4.6	0.62	0.77	-	7	273	65	155	7.35	2.37	-	24.74	2.37	0.80	1.81	-	6.83	0.35	1.38	-	3.23
W05	2	15	16.7	5.6	2.13	1.36	-	5	283	50	140	1.70	2.57	-	9.86	1.70	1.19	2.39	-	6.10	0.63	1.99	-	3.36
W06	3	20	16.7	9.7	7.5	4.2	3.9	5	302	226	316	0.15	0.87	8.67	1.53	0.15	0.15	0.84	4.73	1.52	0.12	0.72	5.96	1.16
W07	2	22	9.2	3.7	0.64	0.8	-	12	324	315	405	-	2.27	2.82	22.86	2.27	0.57	1.55	1.62	2.97	0.34	1.28	2.44	2.21
W08	2	23	12	7.9	2	1.9	-	3	317	332	422	0.76	1.55	11.75	8.99	0.76	0.51	1.40	4.51	5.09	0.29	1.14	6.29	2.84
W09	2	18	8.4	6	0.9	2.5	-	8	60	335	425	0.38	1.48	4.98	2.23	0.38	0.29	1.30	2.87	1.56	0.22	1.12	4.08	1.20
W10	2	23	5.7	3.3	1.3	0.85	-	5	329	313	403	0.30	1.16	7.41	2.53	0.30	0.12	0.71	2.30	0.71	0.11	0.68	5.84	0.75
W11	3	22	1.1	2	0.1	0.64	0.1	4	327	120	210	1.13	1.74	19.08	4.97	1.13	0.12	0.69	2.37	0.51	0.07	0.49	10.57	0.73
W12	2	25	3.9	4	0.74	0.96	-	12	355	297	387	0.64	1.44	2.78	10.36	0.64	0.15	0.82	1.48	1.81	0.14	0.75	2.70	1.61
W13	2	12	11.9	10.9	3	2.28	-	7	36	73	163	1.06	2.77	7.28	9.39	1.06	0.99	2.71	5.63	9.02	0.70	2.41	4.93	5.65
W14	3	19	13	5	0	1.1	0	8	296	73	163	-	2.67	6.40	12.57	2.67	3.75	2.28	3.09	5.15	0.68	1.75	4.41	2.94
W15	2	18	22	6	8.3	0	-	8	351	200	290	0.70	1.84	9.74	2.93	0.70	0.60	1.75	5.03	2.83	0.39	1.50	5.79	2.34
W16	3	11	5.2	7.6	0	2.9	0	13	42	144	234	1.09	3.04	3.46	3.65	1.09	1.01	2.96	2.84	3.45	0.62	2.45	2.98	2.45
W17	3	7	8	2	0	0.56	0	20	30	156	246	7.71	6.72	3.07	6.83	3.07	3.40	5.87	2.29	4.49	1.48	4.70	2.81	2.86
W18	2	12	8.5	4.5	1.61	1.27	-	2	252	253	343	0.97	2.66	20.49	7.05	0.97	0.75	2.46	10.06	4.50	0.50	2.08	8.90	2.82
W19	2	15	4.2	5.2	1.6	0.68	-	5	28	56	146	0.75	2.12	8.71	5.49	0.75	0.48	1.80	4.17	3.66	0.31	1.48	5.79	2.24
W20	3	15	1.8	1.7	0.23	0.5	0.3	4	20	63	153	7.96	2.95	9.44	6.08	2.95	0.29	1.43	3.39	0.87	0.18	1.07	7.12	1.03
W21	3	20	18.9	9	0	2	0	7	348	71	161	-	2.51	4.96	12.25	2.51	-	2.36	3.31	7.48	1.15	1.90	3.58	3.95
W22	2	7	5.4	5.7	1	1.65	-	6	294	53	143	1.53	4.48	-	5.78	1.53	1.44	4.38	-	5.37	1.00	3.81	-	3.88

Note: ~~( ) means the value is not existing. NS Natural scenarios, RS Rainfall scenarios, ES Earthquake scenarios~~ When there is no tensile stress in the mudstone foundation, Fos_{te} has no value. For the case of an anaclinal slope, blocks do not slide and Fos_{sl} has no value. Both parameters are replaced by "-".

5 Discussion

5.1 Characteristics of rock block stability~~Distribution Characteristics of Fos~~

There are up to 12 results of Fos per potential unstable block with the consideration of three scenarios and four failure modes (i.e., partial damage and overall failure). Most ~~of~~ Fos_{te} values are less than 1 in ~~any~~ all scenarios (purple points in Fig.10), except for two blocks (i.e., W17 and W20), whose Fos_{te} values are also close to 1 under rainfall or earthquake scenarios. Although most of Fos_{co} values (green points in Fig. 10) are greater than 1, they are closer to the critical state of $Fos = 1$ than Fos_{sl} and Fos_{to} (represented by blue and yellow points in Fig. 10, respectively). The compression damage of the exposed mudstone can be investigated in the field survey (Fig. 4d). However, it is difficult to observe the phenomenon of tensile damage inside the mudstone base. In the case of weak tensile strength, the mudstone base suffers from tensile failure, and compression failure usually occurs before tension failure. According to the results, their Fos_{te} and Fos_{co} are less than 1 or close to 1, which means that the underlying mudstone has been partially damaged due to slight compressive or tensile failure, and the blocks are potentially unstable with the current depth of the basal cavity. However, most of the blocks do not exhibit ~~the~~ overall failure, and they still exist on the slope. ~~Meanwhile~~Moreover, their Fos_{sl} and Fos_{to} values are greater than 1 in different scenarios, which is consistent with ~~the~~ this actuality. ~~Due to the uncertainty of mechanical parameters,~~ The results indicate ~~it is possible~~ that most of the blocks are close to~~in~~ a critical state, in which they are partially damaged but the whole block is still stable.

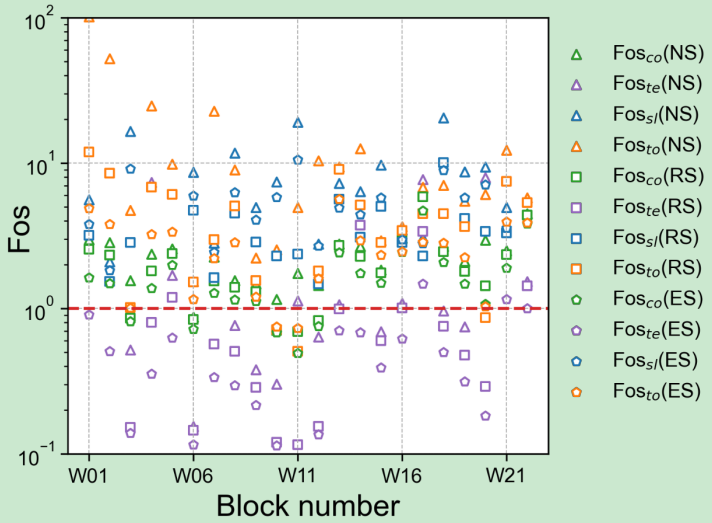

Figure 10 Distribution of Fos in different scenarios. Shapes represent different scenarios and ~~colors~~colours represent different failure modes.

5.2 Relationship between *Fos* and geometric parameters

Fig. 11 presents the relationship between Fos_{min} and two main geometric parameters, the dip of the contact surface and the retreat ratio. In general, the dip angle of the ~~bedding plane~~ contact surface (α) is the key factor influencing the sliding failure mode. The horizontal axis in Fig. 11a is α between the rock blocks and underlying mudstone. Most of the points in Fig. 11a are in the interval [0, 8°], which is consistent with the features of sub-horizontal ~~stratum~~ strata in the study area. The shade of the points does not change significantly in the x-axis direction, as Fig. 11a shows.~~which indicates that the dip of contact surface has little correlation with rockfall stability in this area~~ Therefore, compared with the maximum retreat ratio (r_{max}), the dip of the contact surface has less influence on rockfall stability in the study area. There was a significant positive correlation between the retreat ratio (r_{max}) and Fos_{min}. ~~as Fig. 11b shown.~~ In Fig. 11b, as the retreat ratios increase in the positive direction of the x-axis and y-axis, the rock blocks show a notable tendency to be unstable. ~~all the points can be clearly divided into two parts by a red dashed line, Fos_{min} of the points in the upper part are all lower than the critical state ($Fos = 1$). Therefore, if r_x and r_y can be obtained through the detailed field investigation, the block stability can be preliminarily determined by the formula in the Fig. 11b.~~

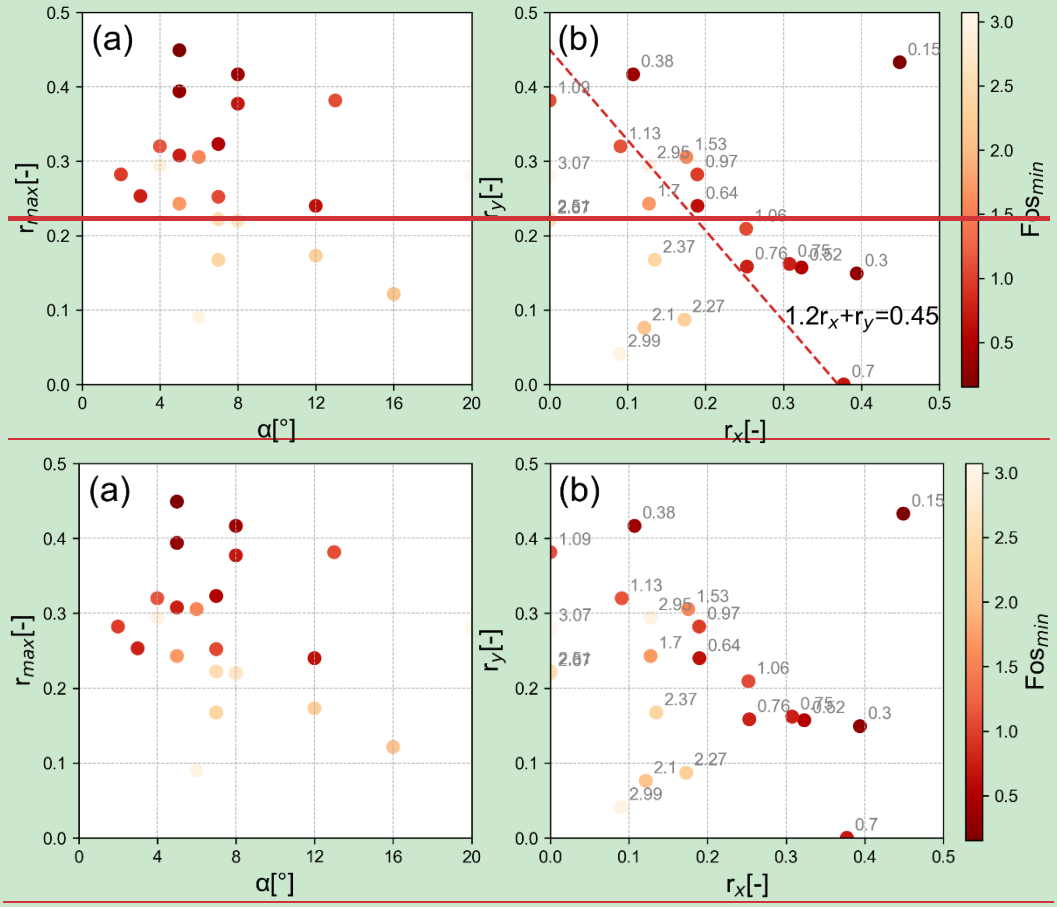

(a)
(b)
α[°]
r_{max}[-]
r_x[-]
r_y[-]
Fos$_{min}$
0.38
1.09
1.13
2.95
1.53
0.97
3.07
1.7
0.64
1.06
2.37
0.76
0.3
2.1
2.27
2.99
0.7
0.15

Figure 11 ~~The relationship~~ Correlation between Fos and ~~main geometric parameters~~ the dip of contact surface and retreat ratio. Here, α is the dip angle of the contact surface between rock block and underlaying mudstone~~.~~ , r_x and r_y are the retreat ratio along x direction and y direction, respectively, equal to d_1/a and d_2/b, and~~,~~ r_{max} is the larger ~~one~~ of r_x and r_y.

5.3 Definition of rockfall susceptibility

~~In order t~~To explore the variation ~~of~~ in Fos with the progressive erosion process of the cavity on the blocks, the cavity retreat velocities in different directions are assumed to be equal (5 mm/year, Zhang et al. (2016)). ~~The rockfall evolution also can be well displayed from Fig. 12.~~ Fig. 12 shows the variations in Fos of two specific blocks during the evolution process of the mudstone cavity.~~The instability of the blocks starts from the failure (or damage) of the foundation.~~ In the initial stage, the cavity is small, and the overlying block is stable; all Fos values are greater than 1.0. The cavity expands over time as the mudstone weathers; then, the contact area decreases, and non-uniform distributed stress arises. When the stress exceeds the ultimate strength of mudstone in a partial area, Fos_{co} and Fos_{te} decrease significantly, as shown in Fig. 12. The instability of the blocks starts from the failure (or damage) of the foundation. Fos_{te} and Fos_{co} reach the critical state much earlier than Fos_{sl} and Fos_{to}. For these two specific blocks, when r_{max} increases to 0.4, Fos_{sl} and Fos_{to} are still higher than 1.0. This means that the rock blocks can remain globally stable in this condition.

These results further elucidate the stability analysis model proposed in this study. Fos_{co} and Fos_{te} introduced in this model present the damage state of basal mudstone caused by compressive and tensile stresses, which do not provide global instability of the overlying block as sliding and toppling. However, Fos_{co} and Fos_{te} are important preliminary signs of subsequent global failure of the rock block. The damage in the basal mudstone can significantly accelerate weathering and prompt expansion of the cavity, which will lead to global failure. The lower Fos_{co} and Fos_{te} are, the lesser the safety margin of the blocks. Therefore, the four Fos used in this study can provide a more comprehensive quantification of rockfall stability.

This result is consistent with Fig. 10, in which ~~90.9%~~63.7% of the purple and green points (Fos_{te} and Fos_{co}-) are ~~near the line of $Fos = 1$~~ located between $Fos = 0.7$ and $Fos = 2.0$. This result ~~also well agrees with the field insight, that is most rock blocks are potential unstable and many fractures appear in the mudstone~~ can be validated by the field phenomena. In the study area, rock damage (e.g., micro-fractures and cleavages) can be observed in the underlying mudstone. However, most overlying rock blocks are stable at the present time. This means that ~~E~~even if Fos_{sl} or Fos_{to} is higher than 1, ~~in fact~~ its foundation has begun to be damaged. In the case of heavy rain or earthquakes, Fos_{sl} and Fos_{to} may be reduced to less than 1, and the rockfall ~~will~~ occurs.

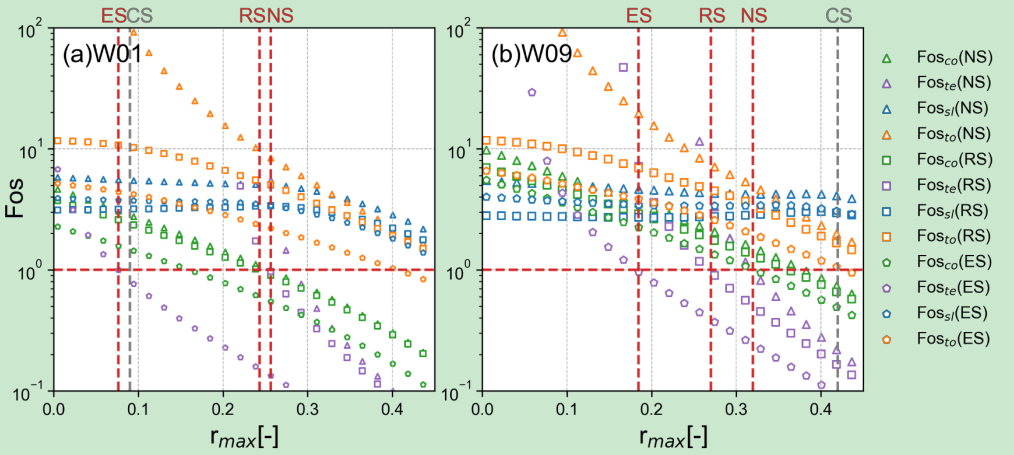

Figure 12 Variation ~~of~~ in Fos with r_{max}. (a) and (b) are the results for W01 and W09, respectively, which represent the situation of the blocks with two and three free faces. The ~~gray~~grey dotted line (CS) approximately represents the current state of the unstable blocks. The red dotted lines correspond to the critical values of r in different scenarios.

Based on the ~~above analysis~~ meaning of four Fos, rockfall susceptibility can be divided into three levels. When both Fos_{co} and Fos_{te} are greater than 1, the overall rock block is stable, and the mudstone base is not damaged, which is defined as "low susceptibility" and represented by the green area in ~~the~~ Fig. 13. With the development of ~~the~~ cavity erosion, when Fos_{co} or Fos_{te} is less than 1 and Fos_{sl} and Fos_{to} are higher than 1, the base ~~begins to~~undergoes be damaged, and the overlying sandstone blocks ~~still maintain~~remain relatively stable. This state is defined as "moderate susceptibility" and represented by the orange area. When Fos_{sl} or Fos_{to} is less than 1 in some scenarios, the rock blocks are in a "high susceptibility" state, which means that rockfalls are highly likely to occur. Fig. 13a indicates that along with the increase ~~of~~ in the cavity retreat ratio, the susceptibility of W01 and W09 changes from low susceptibility to moderate susceptibility in the natural scenario. As Fig. 13b and c show~~n~~, when rainfall or earthquake occurs, Fos_{sl} or Fos_{to} of some blocks ~~are~~ is less than 1, which means that some blocks have evolved to the state of high susceptibility and the overall sandstone blocks are unstable.

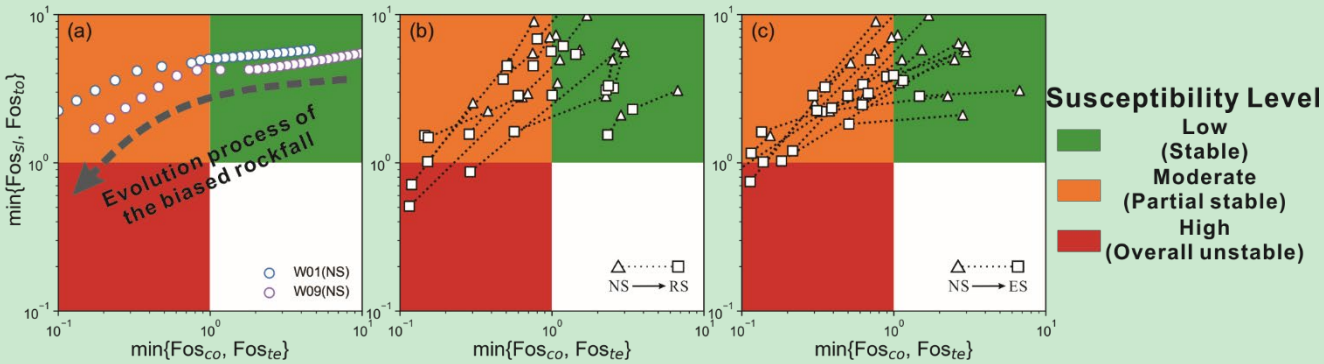

Figure 13 Rockfall susceptibility based on the combination of four Fos ~~distribution~~. The susceptibility is defined as three levels, represented by red, orange and green ~~respectively~~. (a) shows the progressive failure process of the rock block changing from low

susceptibility to moderate susceptibility~~,~~ as the ~~increase of~~ cavity retreat ratio increases (illustrated by W01 and W09 in the natural scenario. (b) and (c) show the change ~~of~~ in susceptibility of biased rock blocks, when the scenario changes from natural conditions to rainfall and earthquake conditions.

5.4 Critical retreat ratio in the study area

The cavity plays an important role in the progressive failure process of biased rockfall. ~~In order t~~To ~~analyze~~analyse the effect of the retreat ratio on the stability of rock blocks, all blocks in the study area were selected to calculate~~d~~ their Fos and susceptibility level with the ~~increased~~ increasing r, whose retreat ~~velocity~~ velocities in different directions are assumed to be equal. Fig. 14 shows that along with the increase ~~of~~ in the retreat ratio, the susceptibility level of rock blocks changes from low to moderate susceptibility. Corresponding to the critical state of $\min\{Fos_{co}, Fos_{te}\} = 1$ of all blocks, the minimum retreat ratio is 0.2~~6565~~, and the maximum retreat ratio is 0.4~~1050~~, ~~which are~~ as marked by the vertical ~~gray~~grey dotted line in ~~the~~ Fig. 14. According to the ~~statistics~~ statistical analysis of critical retreat ratios, both ~~the~~ mean and median are 0.33~~18 and 0.3308, respectively~~. Therefore, the critical retreat ratio~~rate~~ of the rock blocks in the study area ~~is~~ can be determined ~~to be~~as 0.33, which is marked by the vertical red dotted line in the Fig. 14. ~~This result could provide evidence for field investigation and regional risk control of biased rockfall.~~ The critical retreat ratio calculated by this method can be used for the preliminary identification of potential unstable rock blocks in a specific area, which can help concentrate limited risk treatment resources on these priorities.~~The rock blocks with a retreat ratio exceeding 0.33 can be regarded as probable rockfall source, which should be prevented with the highest priority. For unstable rock blocks in sub-horizontal formation, filling the cavity with a support structure is an effective mitigation measure.~~ It should be emphasized that the mechanical parameters and analysis scenarios significantly affect the critical value. Therefore, the elaborative risk control of a given rockfall should be arranged based on its specific parameters and analysis scenarios.

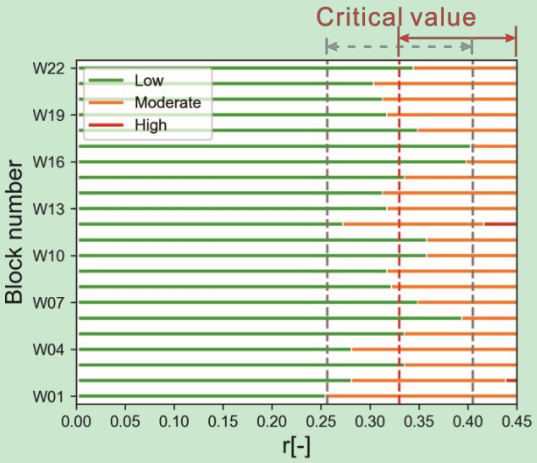

Figure 14 ~~The e~~Effect of the retreat ratio (r) on the Fos of the rock block, which is illustrated by all blocks in the study area. ~~The critical value of r is 0.33.~~

5.5 Limitations

This study involves the development of an analytical model for the three-dimensional stability of biased rockfall, combining the basic LEM method and the consideration of the eccentricity effect. Due to the complexity of rock structure and force analysis, it is necessary to highlight the limitations of this model.

First, this study uses a three-dimensional coordinate system and bending theory. It is difficult to consider diverse shapes of rock blocks, and the rock block was simplified as a prismatic column. The assumption of fully persistent discontinuities may underestimate the stability of rock blocks, and ignores the stress transmission in joints or rock bridges. Then, following the basic framework of the general LEM method, this study assumed that the rock is not subjected to deformations. The complete stress–strain behaviour, such as the deformation in the mudstone layer, is not considered in this study. Furthermore, the block stability is strongly influenced by the uncertainty of mechanical parameters. However, because of the difficulties in sampling strongly weathered mudstone, it is difficult to obtain adequate parameter values for uncertainty statistics. These limitations will be important considerations in future studies.

6 Conclusion

~~Rockfall usually causes amounts of monetary damage and death in mountainous area. For the biased rockfall in sub-horizontal formations, the traditional LEM method usually overestimates the stability of rock blocks with natural cavities.~~ Due to differential weathering in sub-horizontally interbedded of hard rock and soft rock, multi-layer biased rockfalls develop on steep slopes. In mountainous ranges, cut slopes, and coastal cliffs, rockfall may cause significant facility damage and casualties in residential areas and transport corridors. The aim of this study was to present a new three-dimensional analytical method for the stability of rock block~~s~~ with basal ~~cavity~~cavities. ~~In the geological model,~~ In this method, a non-uniform distributed ~~force~~ stress due to the eccentric~~ity~~ effect is applied at the contact surface~~, in place of~~ instead of a point force. The method considers four failure modes according to the rockfall evolution process, including partial damage of the soft foundation (Fos_{co} and Fos_{te}) and overall failure of the rock block (Fos_{sl} and Fos_{to}).

Taking the northeast edge of the Sichuan Basin in Southwest China as the study area, ~~T~~the proposed method ~~was~~ is used to calculate the Fos of ~~the typical unstable rock blocks in the study area~~ biased unstable rock blocks. The results ~~are consistent with the natural states of the rock blocks~~ show that in the natural scenario, the underlying mudstone of some rock blocks has been partially damaged, and compression failure of the mudstone has been observed in the field. Some rock blocks are expected to fail as a whole in rainfall or earthquake scenarios. ~~Besides, t~~The statistical analysis indicates that the retreat ratio is the crucial factor influencing the Fos of biased rockfall. On the basis of different combinations of four Fos, rockfall susceptibility was classified into three levels. As the retreat rate increases, the rock blocks undergo an evolution process from stability to partial instability and then overall instability. Based on the current mechanical parameters of the eastern Sichuan Basin, ~~T~~the critical retreat ratio from low to moderate rockfall susceptibility is 0.33.

The proposed method improves the three-dimensional ~~geo~~mechanical model of a rock block with a basal cavity~~,~~ by considering non-uniform distributed ~~force~~ stress at the contact surface, which could promote the accuracy of rockfall stability analysis. ~~However,~~ Due to the assumptions adopted and ~~because of~~ the complexity of ~~mechanical~~ the failure mechanism of biased rockfall~~ and the assumptions adopted in the method~~, ~~it is essential to highlight the limitations of this method. In the proposed method, the contact surface between rock block and underlying mudstone is assumed to be a rectangle. However, in reality its natural shape is irregular, which results in complex distribution of supporting force. In addition, in the geomechanical model, the failure surface of biased rockfall is set to be the contact surface of rock block and mudstone. However, the natural failure surface may be formed along the cleavages in the mudstone, which will lead to the changes in mechanical parameters of stability analysis~~ there are some limitations in this method, mainly including the simplification of boundary conditions and rock deformation. ~~Further research is clearly needed for the improvement of geomechanical model of biased rockfall~~These limitations will be important considerations in future studies.

Data availability

All raw data can be provided by the corresponding authors upon request.

Author contributions

XS, BC and JD planned the campaign; XS and BC performed the field measurements; XS, BC, WW and BL designed and developed the methodology. XS, BC and JD analysed the data; XS and BC wrote the manuscript draft; JD and WW reviewed and edited the manuscript.

Competing interests

The authors declare that they have no conflicts of interest.

Acknowledgements

This research is funded by the National Natural Science Foundation of China (No. 42172318 and No. 42177159). The first author thanks Master Chengjie Luo and Yu Wang for data collection in the field. We also appreciate the assistance of the Research Center of Geohazard Monitoring and Warning in the Three Gorges Reservoir, China.

References

Adrian, I.: Pressures distribution for eccentrically loaded rectangular footings on elastic soils, Proceedings of the 2010 international conference on Mathematical models for engineering science, Tenerife, Spain, 213–216,

Alejano, L. R., Carranza-Torres, C., Giani, G. P., and Arzua, J.: Study of the stability against toppling of rock blocks with rounded edges based on analytical and experimental approaches, Eng. Geol., 195, 172-184, https://doi.org/10.1016/j.enggeo.2015.05.030, 2015.

Alejano, L. R., Ordóñez, C., Armesto, J., and Rivas, T.: Assessment of the instability hazard of a granite boulder, Nat. Hazards, 53, 77-95, https://doi.org/10.1007/s11069-009-9413-0, 2010.

Ashby, J.: Sliding and toppling modes of failure in models and jointed rock slopes, M.S. thesis, Imperial College London University, London, 1971.

Bray, J. W. and Goodman, R. E.: The theory of base friction models, Int. J. Rock Mech. Min. Sci. Geomech. Abstr., 18, 453-468, https://doi.org/10.1016/0148-9062(81)90510-6, 1981.

Budetta, P.: Assessment of rockfall risk along roads, Nat. Hazards Earth Syst. Sci., 4, 71-81, https://doi.org/10.5194/nhess-4-71-2004, 2004.

Budetta, P. and Nappi, M.: Comparison between qualitative rockfall risk rating systems for a road affected by high traffic intensity, Nat. Hazards Earth Syst. Sci., 13, 1643-1653, https://doi.org/10.5194/nhess-13-1643-2013, 2013.

Chau, K. T., Wong, R. H. C., Liu, J., and Lee, C. F.: Rockfall hazard analysis for Hong Kong based on rockfall inventory, Rock Mech. Rock Eng., 36, 383-408, https://doi.org/10.1007/s00603-002-0035-z, 2003.

Chen, H. K. and Tang, H. M.: Stability analysis method of perilous rock in source of avalanche, J. Geol. Min. Res., 2, 60-67, https://doi.org/10.5897/JGMR.9000070, 2010.

Chen, H. K., Xian, X. F., Tang, H. M., and Feng, Q. H.: A massive development mechanism and countermeasures for perilous rocks in the Three Gorges Reservoir area of PR China: The example of the Taibaiyan cliff at Wanzhou, Journal of Chongqing University, 31, 1178-1184, https://doi.org/10.11835/j.issn.1000-582X.2008.10.019, 2008.

Corominas, J., Mavrouli, O., and Ruiz-Carulla, R.: Magnitude and frequency relations: are there geological constraints to the rockfall size?, Landslides, 15, 829-845, https://doi.org/10.1007/s10346-017-0910-z, 2018.

Cruden, D. M. and Varnes, J. D.: Landslide types and processes. Landslides: investigation and mitigation, transportation research board (National Research Council), National Academy Press, Washington, DC, 1996.

D'Amato, J., Hantz, D., Guerin, A., Jaboyedoff, M., Baillet, L., and Mariscal, A.: Influence of meteorological factors on rockfall occurrence in a middle mountain limestone cliff, Nat. Hazards Earth Syst. Sci., 16, 719-735, https://doi.org/10.5194/nhess-16-719-2016, 2016.

Derron, M. H., Jaboyedoff, M., and Blikra, L. H.: Preliminary assessment of rockslide and rockfall hazards using a DEM (Oppstadhornet, Norway), Nat. Hazards Earth Syst. Sci., 5, 285-292, https://doi.org/10.5194/nhess-5-285-2005, 2005.

Ferrari, F., Giacomini, A., and Thoeni, K.: Qualitative Rockfall Hazard Assessment: A Comprehensive Review of Current Practices, Rock Mech. Rock Eng., 49, 2865-2922, https://doi.org/10.1007/s00603-016-0918-z, 2016.

Frattini, P., Crosta, G., Carrara, A., and Agliardi, F.: Assessment of rockfall susceptibility by integrating statistical and physically-based approaches, Geomorphology, 94, 419-437, https://doi.org/10.1016/j.geomorph.2006.10.037, 2008.

Frayssines, M. and Hantz, D.: Modelling and back-analysing failures in steep limestone cliffs, Int. J. Rock Mech. Min. Sci., 46, 1115-1123, https://doi.org/10.1016/j.ijrmms.2009.06.003, 2009.

Guzzetti, F., Reichenbach, P., and Wieczorek, G. F.: Rockfall hazard and risk assessment in the Yosemite Valley, California, USA, Nat. Hazards Earth Syst. Sci., 3, 491-503, https://doi.org/10.5194/nhess-3-491-2003, 2003.

Hutchinson, J. N.: Field and laboratory studies of a fall in Upper Chalk cliffs at Joss Bay, Isle of Thanet, in: Stress-Strain Behaviour of Soils, Proceedings of the Roscoe Memorial Symposium, Oxfordshire, 29-31 March 1971, 692-706, 1972.

Jaboyedoff, M., Baillifard, F., Philippossian, F., and Rouiller, J. D.: Assessing fracture occurrence using "weighted fracturing density": a step towards estimating rock instability hazard, Nat. Hazards Earth Syst. Sci., 4, 83-93, https://doi.org/10.5194/nhess-4-83-2004, 2004.

Jaboyedoff, M., Ben Hammouda, M., Derron, M.-H., Guérin, A., Hantz, D., and Noel, F.: The Rockfall Failure Hazard Assessment: Summary and New Advances, in: Understanding and Reducing Landslide Disaster Risk: Volume 1 Sendai Landslide Partnerships and Kyoto Landslide Commitment, edited by: Sassa, K., Mikoš, M., Sassa, S., Bobrowsky, P. T., Takara, K., and Dang, K., Springer International Publishing, Cham, 55-83, https://doi.org/10.1007/978-3-030-60196-6_3, 2021.

Kogure, T., Aoki, H., Maekado, A., Hirose, T., and Matsukura, Y.: Effect of the development of notches and tension cracks on instability of limestone coastal cliffs in the Ryukyus, Japan, Geomorphology, 80, 236-244, https://doi.org/10.1016/j.geomorph.2006.02.012, 2006.

Kromer, R., Lato, M., Hutchinson, D. J., Gauthier, D., and Edwards, T.: Managing rockfall risk through baseline monitoring of precursors using a terrestrial laser scanner, Can. Geotech. J., 54, 953-967, https://doi.org/10.1139/cgj-2016-0178, 2017.

Malamud, B. D., Turcotte, D. L., Guzzetti, F., and Reichenbach, P.: Landslide inventories and their statistical properties, Earth Surf. Process. Landf., 29, 687-711, https://doi.org/10.1002/esp.1064, 2004.

Matasci, B., Stock, G. M., Jaboyedoff, M., Carrea, D., Collins, B. D., Guerin, A., Matasci, G., and Ravanel, L.: Assessing rockfall susceptibility in steep and overhanging slopes using three-dimensional analysis of failure mechanisms, Landslides, 15, 859-878, https://doi.org/10.1007/s10346-017-0911-y, 2018.

Pérez-Rey, I., Muñiz-Menéndez, M., González, J., Vagnon, F., Walton, G., and Alejano, L. R.: Laboratory physical modelling of block toppling instability by means of tilt tests, Eng. Geol., 282, 105994, https://doi.org/10.1016/j.enggeo.2021.105994, 2021.

Pierson, L. A., Davis, S. A., and Van Vickle, R.: Rockfall hazard rating system–implementation manual, Federal Highway Administration (FHWA), Report FHWA—OR-EG-90-01, FHWA, US Department of Transportation, 80 pp., 1990.

555 Sagaseta, C.: On the Modes of Instability of a Rigid Block on an Inclined Plane, Rock Mech. Rock Eng., 19, 261-266,
556 https://doi.org/10.1007/Bf01039998, 1986.
557 Santi, P. M., Russell, C. P., Higgins, J. D., and Spriet, J. I.: Modification and statistical analysis of the Colorado Rockfall
558 Hazard Rating System, Eng. Geol., 104, 55-65, https://doi.org/10.1016/j.enggeo.2008.08.009, 2009.
559 Tang, H. M., Wang, L. F., Chen, H. K., and Xian, X. F.: Collapse sequence of perilous rock on cliffs with soft foundation,
560 Chinese Journal of Geotechnical Engineering, 32, 205-210, 2010.
561 Volkwein, A., Schellenberg, K., Labiouse, V., Agliardi, F., Berger, F., Bourrier, F., Dorren, L. K. A., Gerber, W., and
562 Jaboyedoff, M.: Rockfall characterisation and structural protection – a review, Nat. Hazards Earth Syst. Sci., 11, 2617-2651,
563 https://doi.org/10.5194/nhess-11-2617-2011, 2011.
564 Ward, D. J., Berlin, M. M., and Anderson, R. S.: Sediment dynamics below retreating cliffs, Earth Surf. Process. Landf., 36,
565 1023-1043, https://doi.org/10.1002/esp.2129, 2011.
566 Wu, L. Z., Zhang, L. M., Zhou, Y., Xu, Q., Yu, B., Liu, G. G., and Bai, L. Y.: Theoretical analysis and model test for
567 rainfall-induced shallow landslides in the red-bed area of Sichuan, Bull. Eng. Geol. Environ., 77, 1343-1353,
568 https://doi.org/10.1007/s10064-017-1126-0, 2018.
569 Yu, B., Ma, E., Cai, J., Xu, Q., Li, W., and Zheng, G.: A prediction model for rock planar slides with large displacement
570 triggered by heavy rainfall in the Red bed area, Southwest, China, Landslides, 18, 773-783, https://doi.org/10.1007/s10346-
571 020-01528-x, 2021.
572 Zhan, J., Yu, Z., Lv, Y., Peng, J., Song, S., and Yao, Z.: Rockfall Hazard Assessment in the Taihang Grand Canyon Scenic
573 Area Integrating Regional-Scale Identification of Potential Rockfall Sources, Remote Sens., 14, 3021,
574 https://doi.org/10.3390/rs14133021, 2022.
575 Zhang, K., Tan, P., Ma, G. W., and Cao, P.: Modeling of the progressive failure of an overhang slope subject to differential
576 weathering in Three Gorges Reservoir, China, Landslides, 13, 1303-1313, https://doi.org/10.1007/s10346-015-0672-4, 2016.
577 Zhang, M., Yin, Y. P., and Huang, B. L.: Mechanisms of rainfall-induced landslides in gently inclined red beds in the eastern
578 Sichuan Basin, SW China, Landslides, 12, 973-983, https://doi.org/10.1007/s10346-015-0611-4, 2015.
579 Zheng, L. N., Chen, J. B., Zhou, Q. J., Feng, S. Q., Luo, Y. B., and Shen, P.: Experimental study on bearing capacity of
580 moderately weathered mudstone in Chengdu area, Chinese Journal of Geotechnical Engineering, 43, 926-932,
581 https://doi.org/10.11779/CJGE202105017, 2021.
582 Zhou, C., Yin, K. L., Cao, Y., Ahmed, B., Li, Y. Y., Catani, F., and Pourghasemi, H. R.: Landslide susceptibility modeling
583 applying machine learning methods: A case study from Longju in the Three Gorges Reservoir area, China, Comput. Geosci.,
584 112, 23-37, https://doi.org/10.1016/j.cageo.2017.11.019, 2018.
585 Zhou, Y., Shi, S., Zhang, Y., Cai, Q., Liang, J., and Cheng, Y.: Stability of unstable rock in nearly-horizontal sandstone-
586 mudstone stratum due to enlarged rock-cell, Journal of Engineering Geology, 25, 1220-1229,
587 https://doi.org/10.13544/j.cnki.jeg.2017.05.006, 2017.
588